Title: Structural, mechanical and dielectric properties of $Ba_{0.6}Sr_{0.4}TiO_3$ – the benefits of a colloidal processing approach

Author: A. Kaushal S.M. Olhero P. Antunes A. Ramalho J.M.F. Ferreira

PII: S0025-5408(13)00918-5
DOI: http://dx.doi.org/doi:10.1016/j.materresbull.2013.11.028
Reference: MRB 7160

To appear in: *MRB*

Received date: 13-9-2013
Accepted date: 9-11-2013

Please cite this article as: A. Kaushal, S.M. Olhero, P. Antunes, A. Ramalho, J.M.F. Ferreira, Structural, mechanical and dielectric properties of $Ba_{0.6}Sr_{0.4}TiO_3$ *minus* the benefits of a colloidal processing approach, *Materials Research Bulletin* (2013), http://dx.doi.org/10.1016/j.materresbull.2013.11.028

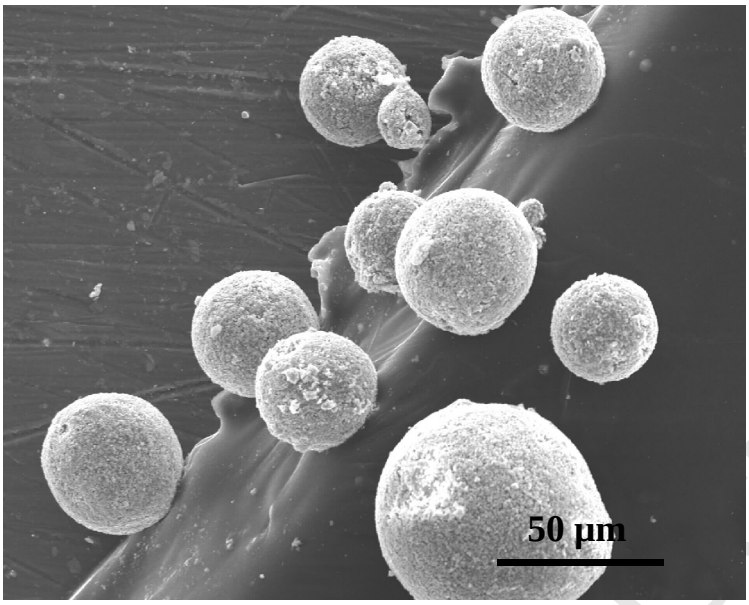

Spherical freeze granules of BST materials

Highlights

- We synthesize micro-sized granules of $Ba_{0.6}Sr_{0.4}TiO_3$ electroceramic material.
- The study disclosed a need of protecting BST powders against hydrolysis.
- An improvement in various properties of BST-FG has been observed.
- Study shows an in-depth understanding of processing electroceramics in water media.

Structural, mechanical and dielectric properties of $Ba_{0.6}Sr_{0.4}TiO_3$ – the benefits of a colloidal processing approach

A. Kaushal[1], S.M. Olhero[1*], P. Antunes[2], A. Ramalho[2], J.M.F. Ferreira[1]

[1]*Department of Materials and Ceramics Engineering, CICECO, University of Aveiro, 3810-193, Aveiro-Portugal*

[2]*Department of Mechanical Engineering, University of Coimbra, Portugal*

Abstract

This paper reports on the benefits gathered from a proper colloidal dispersion/ deagglomeration of a $Ba_{0.6}Sr_{0.4}TiO_3$ (BST) powder in water followed by spraying the aqueous suspension against liquid nitrogen to obtain homogeneous granules. The density of green compacts derived from the freeze granulated (FG) powder was compared with that of compacts prepared from the same starting BST powder but non-granulated (NG). The sintering ability of the greens and the density mechanical and functional properties of the obtained ceramics sintered at various temperatures properties were shown to be strongly enhanced by the freeze granulation step. Freeze granulation enabled decreasing the optimal sintering temperature for 50 ºC, and enhanced all the relevant measured properties, which showed a good correlation with sintered density. Maximum values of dielectric constant ($\varepsilon_{r_{max}} = 5087$) and dielectric loss (tan δ = 0.009) were measured at the phase transition temperature (T_c = -3 ºC) and at a constant frequency of 10 kHz for the FG BST ceramics sintered at 1250 ºC, which also showed a flatter temperature-dependent dielectric profile.

KEYWORDS: A. oxides, A. electronic materials, B. microstructure, B. mechanical properties, D. dielectric properties.

* corresponding author
Email: susana.olhero@ua.pt

1. Introduction

Ferroelectrics are a category of materials with reorientable spontaneous polarization, a sub-category of pyroelectric materials. Because of their high dielectric constant, the electric field dependence and the temperature and frequency dependence of their dielectric constants, ferroelectric materials have a wide range of applications such as IR detection, high-density capacitors, DRAMs, non-volatile ferroelectric memory, and high frequency microwave devices [1-5]. For these applications, barium-strontium titanate solid solutions, $Ba_{1-x}Sr_xTiO_3$ ($0 < x < 1$), have been extensively investigated because they exhibit nonlinear variation of permittivity with the applied electric field within the high frequency range [6-9]. This property offers the opportunity to realize the electrically control of microwave devices. High performance tunable dielectric materials with high dielectric permittivity, low dielectric loss, high dielectric strength, and large nonlinear response to electric field are critical for enhanced precision. Therefore, the development of robust, highly efficient, compact, and powerful electronic devices with wide operational frequency range is an important target.

A key requirement for obtaining materials with superior properties is to control the structural and compositional evolution along all the processing steps. In devices, the ferroelectrics are desired to possess a low dielectric loss and high dielectric constant by applying a relatively low electric field. The primary method of increasing dielectric constant is to make the material dense with less porosity. On the other hand, obtaining enhanced properties at lower costs by decreasing the sintering temperature of the materials is another strategic approach. In recent years, many advances have been made towards producing high quality ceramics by adopting various processing and sintering strategies [10-13]. Dry pressing, the most used conventional method to prepare materials for its large scale commercial applications, requires powders with proper flow and packing behaviours. The inability of dry pressing to destroy particle agglomerates and remove flaws that might exist in

the as-received raw material makes it less suitable to consolidate ceramic components with high reliability for advanced applications. Colloidal shaping methods that enable controlling and manipulating the forces between the particles dispersed in a liquid have attracted the attention of ceramic researchers in the last decades [14–19]. They enable achieving higher microstructural homogeneity in green and sintered parts, while some offer near-net-shaping capabilities that reduce the post sintering machining operations and the production costs. Freeze granulation has shown to be a competitive technique for the manufacture of granules for pressing owing to its ability to preserve the particles homogeneity achieved in the suspension, thus enhancing the pressing performance [20-23]. This technology combines the advantages of colloidal suspensions, spray freezing and freeze drying that offers the possibility to produce very soft, spherical granules which show an excellent flowability that can be compressed to compacts of high homogeneity by simple dry pressing. The formation of hard granules is prevented by this technique that excludes capillary forces during drying. When compared to the traditional spray drying, freeze granulation presents the following advantages: (i) granule density can be controlled by the solid loading of the suspensions; (ii) density and homogeneity are retained (no shrinkage) since no migration of small particles and/or binders are observed; (iii) absence of internal cavities in the granules [20, 23]. The well controlled and self-flowing freeze granulated powders allow automated production of highly dense and defect-free green bodies by relatively quick and simple uniaxial or isostatic pressing methods.

Grain size effects have been also investigated for ferroelectric ceramics prepared by the conventional mixed-oxide processing method and sintered under selected conditions [24-25], or by thin film synthesis [13, 26]. Various researchers have studied the effect of grain size on the dielectric properties of BST ceramics by varying the sintering temperature. It was established that the relative permittivity increases with grain size decreasing down to 0.8 μm

[24, 25, 27-30]. Submicron and/or composite powders require adequate preparation to achieve a pressing performance that ensures dense compaction into a homogeneous state.

In the present work, an attempt has been made to improve the various properties of BST ceramics consolidated from a freeze granulated powder derived from a well dispersed colloidal suspension. The starting BST powder was successfully synthesized via solid state reaction, milled and surface treated against hydrolysis to form stable aqueous suspensions. The dry packing performance of freeze dried granules was compared with that of the same, but non-granulated BST powder. Our study revealed that freeze granulation allows good particle packing, and the sintering of BST deprived of sintering aids to occur at relatively lower temperatures and the obtaining of BST ceramics with enhanced structural, mechanical and dielectric properties.

2. Experimental Procedure

2.1 Synthesis of micro-sized BST granulars

BST powders with chemical formula $Ba_{0.6}Sr_{0.4}TiO_3$ were prepared by the conventional solid state reaction method. High purity $BaCO_3$ (Barium Carbonate, Sigma-Aldrich, Steinheim, Germany, ≥ 99 %), $SrCO_3$ (Strontium Carbonate, Sigma-Aldrich, Steinheim, Germany, ≥ 99.9 %) and TiO_2 (Titanium IV Oxide, Riedel-de Haen, Sielze, Germany, ≥ 99 %) were mixed in the appropriate molar ratios and ground thoroughly by dry milling for 2 h to enhance homogenization and then heat treated at 1150 ºC for 2 h. The calcined material was dry ball-milled for further 2 h and submitted to a second heat treatment for 2 h at 1250 ºC. The as obtained BST powder was attrition milled for 10 h in ethanol followed by drying at 110 ºC, and subsequently surface treated according to a method described elsewhere [31] in order to prevent its reactivity with water when dispersed in aqueous media.

The surface treated BST powder was then dispersed in aqueous media to obtain a suspension with 45 vol.% solids loading using Dispex A–40 (Allied Colloids, Bradford, UK)

as dispersant. To this suspension, about 3 wt.% Duramax D1000 (Rohm and Haas, Lauterbourg, France) relatively to the dry powder was added as an emulsion binder containing 50 wt.% solids. The resultant slurry was then sprayed into liquid nitrogen (−196 ºC) to obtain granules by freeze granulation (Power Pro freeze granulator LS−2, Gothenburg, Sweden) followed by drying at −49 ºC under a pressure of 1×10^{-3} torr in a freeze-drying system (Labconco, LYPH Lock 4.5, Kansas City, MO) for 72 h. The freeze dried granules (FG) were uniaxial pressed into disc-shaped pellets (20 mm diameter, 3−5 mm thickness) and bars (50 mm × 5 mm × 5 mm) at a uniaxial pressure of 60 MPa, followed by isostatic pressing at 200 MPa. To complete the study, BST ceramics were also prepared by the same conventional dry-pressing method and from the same milled, but non-granulated (NG) BST powder with the same added amount of binder. The consolidated shapes and pressure conditions were the same for FG and NG BST samples. Binder removal was performed by heat treating the BST compacts made of FG and NG powders at a heating rate of 1 ºC min^{-1} up to 600 ºC, and holding at this temperature for 1 h. The samples were then heated at a rate of 5 ºC min^{-1} up to different sintering temperatures (1250, 1300, 1350 and 1400 ºC), hold for 4 h at the set temperature, followed by natural cooling.

2.2 Structural characterization of sintered BST materials

The crystallinity of the samples was studied using a Rigaku X-ray diffractometer of CuK_α (1.54 Å) radiations in θ–2θ geometry. Bulk density (ρ_{bulk}) of FG and NG BST ceramics was measured in ethylene glycol liquid media according to Archimedes principle (ASTM C372, ASTM International, West Conshohocken, PA) using a Mettler balance (AG 245, Mettler Toledo, Zurich, Switzerland). Three density measurements were performed for each kind of ceramic sample and the results are expressed as the average with ± 0.01 error. Polished microstructures of sintered ceramics were examined by scanning electron

microscopy (SEM, JSM-5410, JEOL, Tokyo, Japan) with an energy-dispersive scanning attachment (Sigma 3.42 Quaser, Kevex, Stanford, Valencia, CA).

2.3 Mechanical characterization of sintered BST ceramics

2.3.1 Hardness

Vickers micro hardness of the sintered FG and NG BST ceramics was measured using Struers Duramin testing equipment (Struers, Denmark), according to the requirements of the Standard Test Method for Micro-indentation Hardness of Material (ASTM C1327-08, 2008) [32]. Every surface was correctly polished prior to the hardness measurement. A load of 0.50 kgf (4.905 Newton) [HV0.5] has been applied for a period of 15 seconds. At least ten indentations were made in each specimen to determine the average hardness and the respective standard deviation.

2.3.2 Impulse excitation of vibration (IEV)

The Young's modulus was determined as described by Braem et al. [33], and according to the standard methodology [34]. For this, each BST ceramic was set in free flexural vibration by a light mechanical impulse. A strain-gage, glued to the ceramic's surface, captured the flexural vibration signal. The fundamental frequency of the first flexural vibration mode was determined analysing the vibration response by Fast Fourier Transform (FFT). Ten impulse excitation signals acquisitions were considered in order to determine through numerical methods the average Young's modulus.

2.3.3 Three point bending

The three point bending tests were conducted in a Shimadzu Autograph AG-X-1kN Universal Testing Machine (Kyoto, Japan), controlled by digital electronics at room temperature (~21ºC) in ambient air. The specimen's dimensions were measured with a digital calliper (Mitutoyo Co., Kawasaki, Japan) before testing. The adopted criterion for failure was the specimen's fracture. The load was applied at a rate of 0.5 mm min^{-1} until failure was

reached. The load *versus* displacement relationship was recorded. Maximum load for failure and stiffness were determined from the load-displacement curves. Considering the scatter of mechanical properties in brittle materials, ten specimens of each sintering temperature samples, were tested under the same conditions to provide sufficient representative information. All tests were performed according to standard ASTM C 1161 – 02c (2008) [35].

2.4 Electrical characterization of sintered BST materials

For the measurement of electric properties, BST ceramics sintered at 1250 ºC and 1300 ºC obtained from NG and FG powders were polished to the thickness of ~0.25 mm. Top conductive electrodes were deposited on both sides using silver paste. The temperature and frequency dependence of the dielectric properties were measured in the range of -123 ºC to 87 ºC and 100 Hz to 2 MHz respectively, by an Agilent 4294A impedance analyser.

3. Results and Discussion

3.1 Structural properties

The high temperature used for the synthesis of BST powders (1250 ºC) promoted the formation of hard agglomerates that had to be destroyed. Attrition milling for 10 h in ethanol revealed to be effective in this pursue and resulted in a final bimodal particle size distribution with an average particle size of ~0.26 μm, but with two particle populations. A bimodal particle population is expected to increase the particle packing ability in the slurry, since the smaller particles could occupy the interstitial spaces between the larger ones and release the liquid immobilised in void spaces [36]. In this way, bimodal particle size distributions enable a decrease in viscosity for a given solids loading, or the use of a higher solids volume fraction while maintaining a given viscosity level, a key point for successfully fabricating high dense granules and enhancing the packing density upon dry pressing. Fig. 1 shows a SEM image of green BST granules obtained after freeze-drying. The granules are spherical and their

diameters are within the range of few tens of micrometres. These morphological/size features confer them free flow behaviour and low friction with die wall upon dry pressing, which are essential for obtaining homogeneous and highly dense BST compacts.

Figure 2 shows the XRD patterns of BST ceramic samples consolidated from the freeze granulated powder (FG) and non-granulated powder (NG) sintered for 4 h at the sintering temperatures (T_{sint}) of 1250, 1300, 1350 and 1400 ºC. All the patterns of both FG and NG BST ceramics exhibit a prominent diffraction (110) peak along with other low intensity peaks corresponding to cubic phase of BST (JCPDS card No. 34-0411). However, for T_{sint} = 1400 ºC, impurity peaks could also be observed at 2θ ~29º which correspond to barium orthotitanate (Ba_2TiO_4) phase (JCPDS card No. 00-038-1481). These impurity peaks are absent in the XRD patterns for FG and NG samples sintered at 1250 and 1300 ºC, indicating that higher sintering temperatures have an undesirable effect on the phase assemblage of BST ceramics. To gain further insight, the crystallite sizes of FG and NG BST ceramics submitted at different T_{sint} were calculated from XRD data using Scherrer's formula [37] given by:

$$d_{hkl} = \frac{0.9\lambda}{\beta_{hkl}\cos\theta_{hkl}} \qquad (1)$$

where λ is the X-ray wavelength, β_{hkl} is the full width at half maximum (FWHM) of the Bragg diffraction on the 2θ scale and θ_{hkl} is the Bragg diffraction angle. Instrumental broadening of 0.10 was incorporated for the size calculations. Table 1 shows that increasing T_{sint} resulted in larger crystallite sizes, probably due to enhanced crystal growth kinetics favoured with rising temperature. Merging smaller crystals into larger ones might also result from potential energy differences between small and large crystals and the associated solid state diffusion as per Ostwald ripening [38]. Interestingly, the crystallite size values determined for FG BST ceramics were found to be always higher in comparison to those measured for NG BST ceramics. The observed differences suggest that the diffusion paths

have been shortened in the samples derived from the FG powder due to their higher degree of homogenisation. Generally, micron-sized granules obtained on freeze granulation have low green density compared to particle density, which favours particles' rearrangements and the elimination of the intergranular pores. The binder in frozen granules acts as lubricant, assisting particles sliding and rearrangement, which increase the packing efficiency and compact density. This explains why the green density of FG compacts is about 3 % higher in comparison to that of NG ones (Table 1).

An increase in green density will enhance the densification ability while implying a decrease of shrinkage upon sintering up to the maximum achievable density. This is confirmed by the data plotted in Fig. 3 that compares the dilatometric curves of FG and NG green bodies measured from room temperature to 1310 ºC. Essentially, horizontal lines can be observed up to ~1000 ºC and ~1150 ºC for FG and NG samples, respectively. These horizontal lines mean that the thermal dilatation of the greens along the lower temperature range has been offset by the porosity of the compacts and by small shrinkage derived, for example, from the binder burnout (small depression centred at ~200 ºC). The benefits of freeze granulation are here very evident, being translated by a downshift of the onset of shrinkage of ~150 ºC. For temperatures above ~1000 ºC and ~1150 ºC, for FG and NG samples, respectively, densification has completely overridden any thermal dilatation, resulting in high shrinkage rates. The slop of the curves then gradually changed upon approaching full density, with slop changes occurring at about ~1260 ºC and ~1288 ºC, for FG and NG samples, respectively. However, above those temperatures the slop is less accentuated in case of FG BST sample, meaning that at ~1260 ºC this sample is closer to full densification than the NG BST sample is at ~1300 ºC. These observations are in good agreement with density data reported in Table 1.

As a matter of fact, Table 1 reveals that a maximum relative density of ~99.6 % (based on the theoretical density of BST = 5.41 g cm^{-3} measured by helium pycnometry) for the FG BST was achieved at the lowest sintering temperature tested (1250 ºC), followed by a decreasing trend to ~96 % (1300 ºC) and to ~91 % (1400 ºC). In the case of NG BST ceramics, the relative density at 1250 ºC was significantly lower (~94 %) in comparison to that of FG BST counterpart sintered at the same temperature, but then increased to a maximum of ~99 % at 1300 ºC, followed by a decreasing trend to ~95 % with further increasing the sintering up to 1400 ºC due to an over firing effect. These results are very consistent with the dilatometry curves shown in Fig. 3, confirming that freeze granulation enhances densification and enables achieving almost full densification (~99.6 %) at a temperature that is ~50 ºC lower in comparison to that required (1300 ºC) to promote a slightly lower maximum densification degree (~99 %) in the case of NG BST ceramics. Grain growth is also expected to be faster along the last sintering stage, which is achieved earlier in the case of FG BST ceramics. This explains the larger crystallite sizes measured for these ceramics (Table 1), and the enhanced intensity of the respective XRD peaks (Fig. 2). All these features support the enhanced densification ability of the FG BST powder.

On the other hand, both FG and NG BST samples experienced similar total weight loss of ~4 wt.% up to 1300 ºC (Table 1), ~1.5 wt.% of it attributable to the binder burnout and the remaining to the release of some free water and OH/CO_2 groups adsorbed to the surface of the particles. Further increasing the sintering temperature enhanced the weight loss, likely due to the volatilization of some species. The clear identification of the Ba_2TiO_4 phase for the samples sintered at 1400 ºC (Fig. 2), suggests a gradual depletion of Sr-containing species and a concomitant enrichment in Ba-containing species. The release of gaseous species inside a dense body is likely leading to the formation of pores, pores coalescence and volume expansion, with negative consequences on the final density. This is confirmed by the

microstructural changes undergone by FG and NG BST ceramics (Fig. 4) by the decreasing sintered density values upon sintering at temperatures beyond the optimal ones (1250 ºC for FG), and 1300 ºC for NG), Table 1.

Figure 4 also reveals different microstructural evolutions with sintering temperature for the FG and NG BST ceramics. A highly dense microstructure with least porosity has been observed in case of FG BST ceramic sintered at 1250 ºC, whereas a large number of pores can be observed for NG BST ceramics sintered at the same temperature. A high degree of densification is apparent for the NG BST ceramics sintered at 1300 ºC, coexisting with a few larger pores, indicating that pores coalescence has already started. However, this phenomenon is more evident in case of FG BST ceramics for T_{sint} ≥1300 ºC, being in good agreement with density data reported in Table 1 and the dilatometric curves displayed in Fig. 3. These results confirm that all the thermal events occur at lower temperatures for ceramics consolidated from FG powders than ceramics consolidate from NG powders due to their enhanced homogeneity.

3.2 Mechanical characterization

The effects of processing parameters [freeze granulated *versus* non-granulated BST powders, and sintering temperature (1250, 1300 and 1350 ºC)] on the mechanical properties of BST ceramics were also investigated. The values of dynamic Young's modulus (E) of the FG and NG BST ceramics sintered at different T_{sint} were calculated as a function of frequency of the first flexural vibration mode using Eq. 1:

$$E = 0.9465\left(\frac{mf_t^2}{d}\right)\left(\frac{l^3}{t^3}\right)T_1 \qquad (1)$$

where, l and d are the length and width of the ceramic bar, m is their mass and f_t is the fundamental frequency [39]. T_1 is a correction factor to take into account the finite dimensions of BST ceramic bars (as per ASTM C1259-96 standards).

Fig. 5a reveals that maximum hardness (H) values were measured for the BST ceramics sintered at 1250 ºC (FG, H ~8100 MPa) and at 1300 ºC (NG, H ~7000 MPa), which were then followed by clear decreasing trends with further increasing T_{sint} to higher values. Similar evolutions could be observed for the elastic moduli (Fig. 6a, Table 2). Such variations of the mechanical properties with T_{sint} mean that for the NG BST ceramics, the optimal (but lower) values could only be achieved at a T_{sint} that is ~50 ºC higher than that required to confer the highest mechanical performance to the FG BST ceramics. The observed variations in mechanical properties scale well with sintering density values, being in good agreement with the sintered microstructures presented shown in Fig. 4. The hardness *versus* density fittings shown in Fig. 5b could be described by the following linear equations, $y = 632.16x - 55156$ (correlation factor R^2 ~ 0.98) and $y = 468.2x - 39451$ (correlation factor R^2 ~ 0.97) for FG and NG BST ceramics, respectively. Similar linear correlations were found for the elastic properties (static modulus) *versus* density as revealed in Fig. 6b.

Table 2 presents various mechanical parameters calculated from three point bending strength and IEV test for both FG and NG BST ceramics sintered at different T_{sint}. It can be seen that a good correlation exists between the dynamic and static Young's moduli, meaning that the non-destructive technique can be safely used to assess and the elastic properties of BST ceramics. Again, the maximum values of dynamic and static Young's moduli were registered for FG BST ceramics sintered at 1250 ºC, whereas in the case of NG BST the maximum values were measured for the ceramics sintered at 1300 ºC. As mentioned above, this behaviour is in co-relation with the degree of densification achieved upon sintering. Work of fracture represents the energy absorbed in the fracture failure process of the BST sample under the flexural tests. A small variation in the calculated values of work of fracture as shown in Table 2 indicates a small toughness sensibility of BST material with the T_{sint}. NG BST ceramics show smaller work of fracture values compare to those obtained for FG BST ceramics. Globally the calculated parameters are higher for FG BST specimens, in good consistency with the main trends observed; confirming that freeze granulation enhances the density and microstructural uniformity of the sintered bodies and, consequently, their mechanical reliability.

3.3 Electrical properties

For the electrical characterization, namely dielectric constant (ε_r) and dielectric loss (tan δ), the sintering conditions (1250 ºC and 1300 ºC) that enabled achieving the best physical properties for the BST ceramics were chosen. The temperature dependences of ε_r and tan δ within the range from -123 ºC to 87 ºC at 10 kHz are shown in Fig. 7a and Fig. 7b, respectively. It can be seen that all the evaluated ceramics exhibit a maximum dielectric constant ($\varepsilon_{r_{max}}$) at -3 ºC, corresponding to the transition from ferroelectric to paraelectric (tetragonal to cubic) phase for $B_{0.6}Sr_{0.4}TiO_3$ composition. The temperature dependent ε_r of FG BST ceramics displays a flatter profile in comparison to that of NG BST ceramics,

indicating better stability over a wide temperature range. Moreover, $\varepsilon_{r_{max}}$ value of 5087 has been measured for FG BST sintered at 1250 ºC whereas $\varepsilon_{r_{max}}$ value decreased to 4528 for NG BST sintered at the same temperature. On the other hand, the tan δ *versus* T plots (Fig. 7b) show lower tan δ values for ceramics consolidated from the FG BST powder in comparison to those consolidated from the NG BST powder. The decrease in tan δ can be attributed to the enhanced homogeneity of BST ceramics derived from the FG powder due to the higher compaction degree of the green bodies and their better sintering ability in comparison to those derived from the NG BST powder.

These results indicate that dielectric properties are also closely related with density and microstructural features of sintered ceramics, which, in turn depend on the experimental processing variables. Freeze granulation of the starting BST powder has an overall positive impact on green and sintered properties. This is also confirmed for the measured values dielectric properties, $\varepsilon_{r_{max}}$ and tan δ, for FG and NG BST ceramics sintered at 1250 ºC and 1300 ºC, as presented in Table 3.

The frequency dispersions of the ε_r and tan δ values of FG and NG BST ceramics measured at T_c = -3 ºC within the range from 100 Hz to 2 MHz are shown in Fig. 8a and Fig. 8b, respectively. All the ceramics exhibit minimal dispersion of ε_r and tan δ as a function of the frequency. It is also clear that for both FG and NG BST ceramics, tan δ increases with increasing T_{sint}. Moreover, samples consolidated from NG BST powders show higher tan δ values than those consolidated from FG BST powders (Table 3). For example, along the whole measuring frequency range (100 Hz – 2 MHz), FG 1250 ceramic sample shows tan δ values approximately constant to minimum values of tan δ (tan δ = 0.009) whereas higher values of tan δ (minimum tan δ = 0.013) has been observed for the NG 1250 ceramics with a small variations in tan δ values in whole measuring frequency range which reveals better

interfacial characteristics between ceramic and electrode in case of FG 1250 ceramics. Although, NG BST ceramics sintered at 1300 ºC show ε_r values nearly equal to those of FG BST ceramics sintered at 1250 ºC, the tan δ values of the first were found to be quite higher than those of FG 1250 ºC ceramics. The lower values of tan δ measured for FG 1250 ºC ceramics along the whole frequency range up to 2 MHz enable improved figures of merits, as low tan δ with high tunability are required for tunable microwave applications. The data reported in Fig. 7 and Fig. 8 show that BST ceramics consolidated from the freeze granulated powder processing methods improved the dielectric properties. These results are very consistent with the general enhancement observed in all physical properties.

4. Conclusions

Micro-sized BST granules were successfully fabricated via spraying a stable aqueous suspension with a solid loading of 45 vol.% into liquid nitrogen (freeze granulation), followed by freeze drying. From the results obtained it is possible to conclude that green compacts derived from freeze granulated BST powder exhibit enhanced densification ability upon sintering, when compared with that of compacts derived from the same BST powder but non-granulated. Freeze granulation enabled decreasing the maximum density *versus* sintering temperature for at least 50 ºC, enhance the homogeneity of the sintered microstructures and all the relevant mechanical properties. These improvements were positively reflected on electrical properties, dielectric constant (ε_r) and dielectric loss (tan δ). All the relevant physical and electrical properties of BST ceramics revealed good correlations with sintered density, which in turn was shown to be strongly dependent on the quality of the processing translated by the homogeneity of the green compacts.

Acknowledgments

A. Kaushal and S.M. Olhero would like to thanks the Foundation for Science and Technology of Portugal (FCT) for the financial support under the grants SFRH/BPD/77598/2011 and SFRH/BPD/87486/2012, respectively. The authors would also like to thank CICECO for the work at the University of Aveiro and FCT for the financial support under the project PTDC/CTM/099489/2008.

References

[1] D.S. Wuu, R.H. Horng, C.C. Lin, Y.H. Liu, Microelectron Eng 66 (2003) 600-607.

[2] H.V. Alexandru, C. Berbecaru, A. Ioachim, M.I. Toacsen, M.G. Banciu, L. Nedelcu, D. Ghetu, Mater. Sci. Eng. B 109 (2004) 152-159.

[3] G. Arlt, U. Bottger, S. Witte, Appl. Phys. Lett., 63 (1993) 602-604.

[4] R.E. Jones, Solid State Technol. 40 (1997) 201-210.

[5] N. Setter, R. Waser, Acta Mater., 48 (2000) 151-178.

[6] B. Su, T.W. Button, J. Appl. Phys. 95 (2004) 1382-1385.

[7] S.S. Gevorgian, E.L. Kollberg, IEEE Trans. Microwave Theory Tech., 49 (2001) 2117-2124.

[8] F. Zimmermann, M. Voigts, C. Weil, R. Jakoby, P. Wang, W. Monesklou, E. Ivers-Tiffée, J. Eur. Ceram. Soc. 21 (2001) 2019-2023.

[9] C. Berbecaru, H.V. Alexandru, C. Porosnicu, A. Velea, A. Ioachim, L. Nedelcu, M. Toacsan, Thin Solid films, 516 (2008) 8210-8214.

[10] M. Naito, M. Okumiya, H. Abe, A. Kondo, C.C. Huang, KONA Powder and Particle Journal, 28 (2010) 143-154.

[11] Y. Zhao, V. Bedekar, A. Aning, S. Priya, Materials Letters, 74 (2012) 151-154.

[12] S. Yun, X. Wang, D. Xu, Mater. Res. Bull. 43 (2008) 1989-1995.

[13] B. Su, T.W. Button, J. Eur. Ceram. Soc., 21 (2001) 2641-2645.

[14] L. Bergstrom, in: Holmberg K (Eds). Colloidal processing of ceramics, Handbook of Applied Surface and Colloid Chemistry, ISBN 0471 490830, John Wiley & Sons Ltd, New York, 2001, pp. 201-218.

[15] R. Moreno, Advances in Applied Ceramics, 111 (2012) 246-253.

[16] F. Boschini, B. Guillaume, A. Rulmont, R. Cloots, R. Moreno, J. Eur. Ceram. Soc. 26 (2006) 1591-1598.

[17] I. Ganesh, S.M. Olhero, P.M.C. Torres, J.M.F. Ferreira, J. Am. Ceram. Soc. 92 (2009) 350-357.

[18] S.M. Olhero, I. Ganesh, P.M. Torres, J.M.F. Ferreira, Langmuir, 24 (2008) 9525-9530.

[19] S.M. Olhero, I. Ganesh, P. Torres, F.L. Alves, J.M.F. Ferreira. J. Am. Ceram. Soc., 92 (2009) 9-16.

[20] K. Rundgren, O. Lyckfeldt, M. Sjöstedt, Ceramic Industry, 153 (2003) 40-44.

[21] O. Lyckfeldt, D. Käck, K. Rundgren, Ceram. Eng. Sci. Proc., 24 (2003) 331-336.

[22] O. Lyckfeldt, K. Rundgren, M. Sjöstedt, Key Engineering Materials, 2004, 264-268 [Part 1] 281-284.

[23] Q. Wang, S.M. Olhero, J.M.F. Ferreira, W. Cui, K. Chen, Z. Xie, J. Am. Ceram. Soc., 96 (2013) 1383-1389.

[24] N. Bernaben, A. Leriche, B. Thierry, J.C. Niepce, R. Waser, Fourth Euro Ceramics, 5 (1995) 203-210.

[25] H.T. Martirena, J.C. Burfoot, J. Phys. C: Solid State Phys., 7 (1974) 3182-3192.

[26] K. Kinoshita, A. Yamaji, J. Appl. Phys. 47 (1976) 371-373.

[27] K.T. Kim, Chang-II Kim, Thin Solid Films 472 (2005) 26-30.

[28] W. Buessem, L.E. Cross, A.K. Gosmani, J. Am. Ceram. Soc., 49 (1966) 33-35.

[29] W. Buessem, L.E. Cross, A.K. Gosmani, J. Am. Ceram. Soc., 49 (1966) 36-39.

[30] G. Arlt, D. Hennings, G.D. With, J. Appl. Phys. 58 (1985) 1619-1625.

[31] S.M. Olhero, A. Kaushal, J.M.F. Ferreira, J. Am. Ceram. Soc., (submitted).

[32] ASTM standard C1327-08, Standard Test Method for Vickers Indentation Hardness of Advanced Ceramics, DOI: 10.1520/C1327-08, www.astm.org.

[33] M. Braem, P. Lambrechts, V. Van Doren, G. Vanherle, J. Dent. Res., 65 (1986) 648-653.

[34] ASTM standard C1259-08e1, Standard Test Method for Dynamic Young's Modulus, Shear Modulus, and Poisson's Ratio for Advanced Ceramics by Impulse Excitation of Vibration, DOI: 10.1520/C1259-08E01, www.astm.org.

[35] ASTM C1161-02c(2008)e1, Standard Test Method for Flexural Strength of Advanced Ceramics at Ambient Temperature, DOI: 10.1520/C1161-02CR08E01, www.astm.org.

[36] S.M. Olhero, J.M.F. Ferreira, Powder Technology, 139 (2004) 69-75.

[37] B.D. Cullity, S.R. Stock, Elements of X-Ray Diffraction, third ed., Prentice Hall, New Jersey, 2001.

[38] IUPAC, Compendium of Chemical Terminology (Gold Book), second ed., Blackwell science, Cambridge, UK, 1997.

[39] A. Hauert, A. Rossoll, A. Mortensen, Composites Part A: Applied Science and Manufacturing, 40 (2009) 524-529.

Table and Figure captions

Table 1: Calculated values of densities, linear shrinkage, weight loss and crystallite sizes for FG and NG BST samples sintered at different temperatures.

Table 2: Values of dynamic elastic modulus, static elastic modulus, and work of fracture measured for both FG and NG BST ceramics sintered at different T_{sint}.

Table 3: Calculated $\varepsilon_{r_{max}}$ and tan δ values for both FG and NG BST ceramics sintered at 1250 ºC and 1300 ºC, measured at 10 kHz.

Figure 1: SEM image of green BST granules obtained after freeze-drying.

Figure 2: XRD patterns of FG and NG BST ceramics sintered at different T_{sint} of 1250, 1300, 1350 and 1400 ºC.

Figure 3: Dilatometric behaviour of FG and NG BST green compacts from room temperature to 1310 ºC. The insert shows details within the high temperature range (1100–1310 ºC).

Figure 4: SEM images of polished FG and NG BST ceramics sintered at different T_{sint} of 1250, 1300, 1350 and 1400 ºC.

Figure 5: Dependence of hardness on: (a) sintering temperature, and (b) density, for both FG and NG BST ceramics.

Figure 6: Dependence of Young's modulus (static) on: (a) sintering temperature, and (b) density, for both FG and NG BST ceramics.

Figure 7: Dielectric properties of FG BST and NG BST ceramics sintered at 1250 and 1300 ºC as a function of temperature in the range from -123 ºC to 87 ºC at 10 kHz: (a) ε_r and (b) tan δ.

Figure 8: Frequency dispersion of: (a) ε_r and (b) tan δ values of FG and NG BST ceramics, in the range from 100 Hz to 2 MHz measured at T_c = -3 ºC.

Table 1

NG BST ceramic					FG BST ceramic			
ρ_{green} = 54.50 %		Linear shrinkage (%)	Weight loss (%)	Crystallite size (nm)	ρ_{green} = 57.53 %		Linear shrinkage (%)	Weight loss (%)
ρ_{bulk} (g cm^{-3})	$^{*}\rho_{relative}$ (%)				ρ_{bulk} (g cm^{-3})	$\rho_{relative}$ (%)		
5.10	94.3 ± 0.4	12.3 ± 0.2	3.99 ± 0.02	31.43	5.39	99.6 ± 0.4	14.0 ± 0.3	4.04 ± 0.01
5.35	99.0 ± 0.1	14.8 ± 0.1	4.01 ± 0.05	37.16	5.17	95.6 ± 0.4	12.7 ± 0.4	4.01 ± 0.04
5.16	95.4 ± 0.3	13.6 ± 0.1	4.29 ± 0.02	43.05	4.99	92.3 ± 0.1	11.6 ± 0.1	4.40 ± 0.14
5.12	94.6 ± 0.3	13.4 ± 0.2	5.01 ± 0.03	53.60	4.92	90.9 ± 0.1	11.1 ± 0.3	5.32 ± 0.35

*Theoretical value of particle density used for relative density calculation was measured to be 5.41 g cm^{-3} using Multi Pycnometer (Quanta Chrome, USA)

Table 2:

T_{sint} (ºC)	NG BST ceramic			FG BST ceramic		
	Dynamic Elastic Modulus (MPa)	Static Elastic Modulus (GPa)	Work of fracture (J/m^2)	Dynamic Elastic Modulus (MPa)	Static Elastic Modulus (GPa)	Work of fracture (J/m^2)
1250	155.0 ± 6.6	174.6 ± 2.1	0.079 ± 0.003	223.1 ± 3.3	220.2 ± 9.9	0.187 ± 0.057
1300	187.0 ± 3.3	204.0 ± 5.8	0.110 ± 0.002	169.0 ± 1.9	175.7 ± 9.2	0.200 ± 0.042
1350	163.6 ± 7.3	161.6 ± 8.4	0.068 ± 0.008	166.9 ± 5.3	179.1 ± 0.7	0.186 ± 0.013

Table 3:

Samples	$\varepsilon_{r_{max}}$	tan δ
FG 1250	5087	0.009
NG 1250	4528	0.013
FG 1300	4856	0.025
NG 1300	5034	0.042

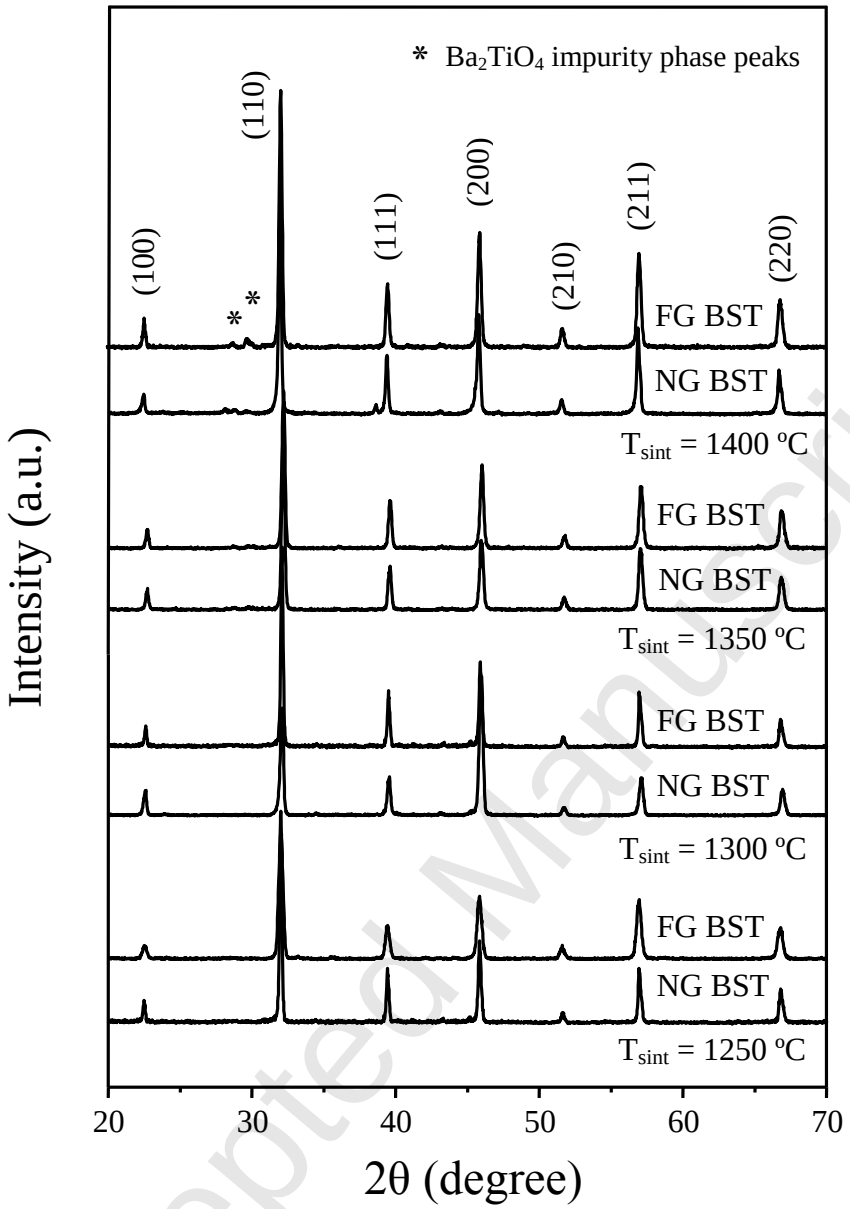

Figure 2

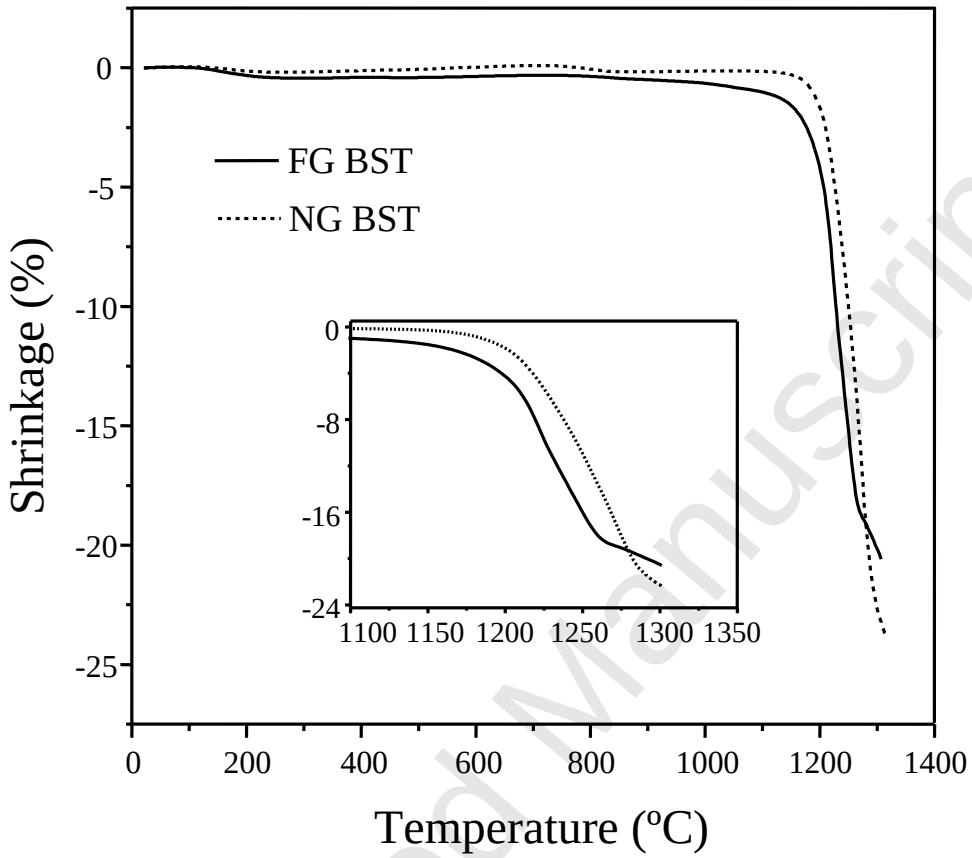

Figure 3

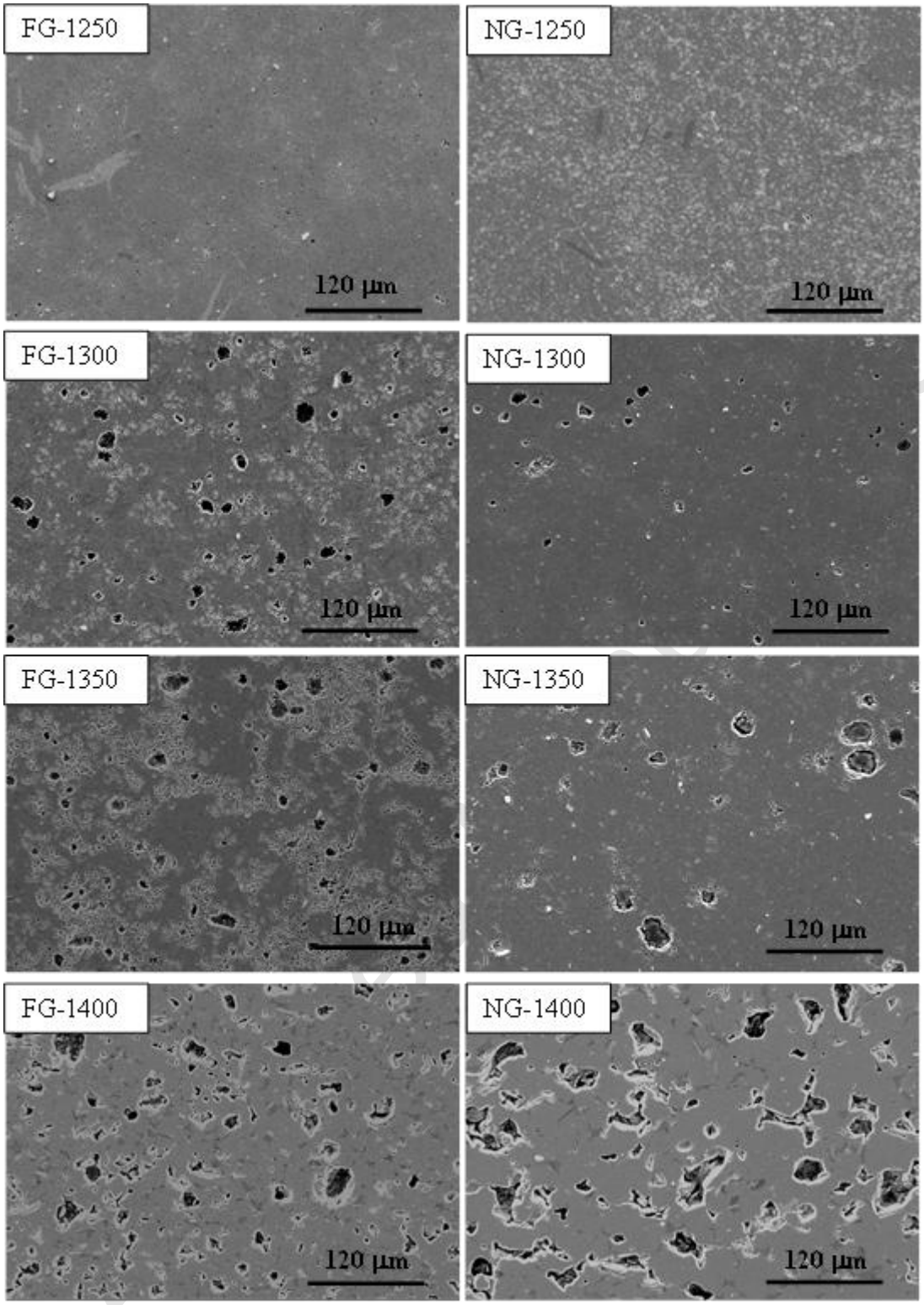

Figure 4

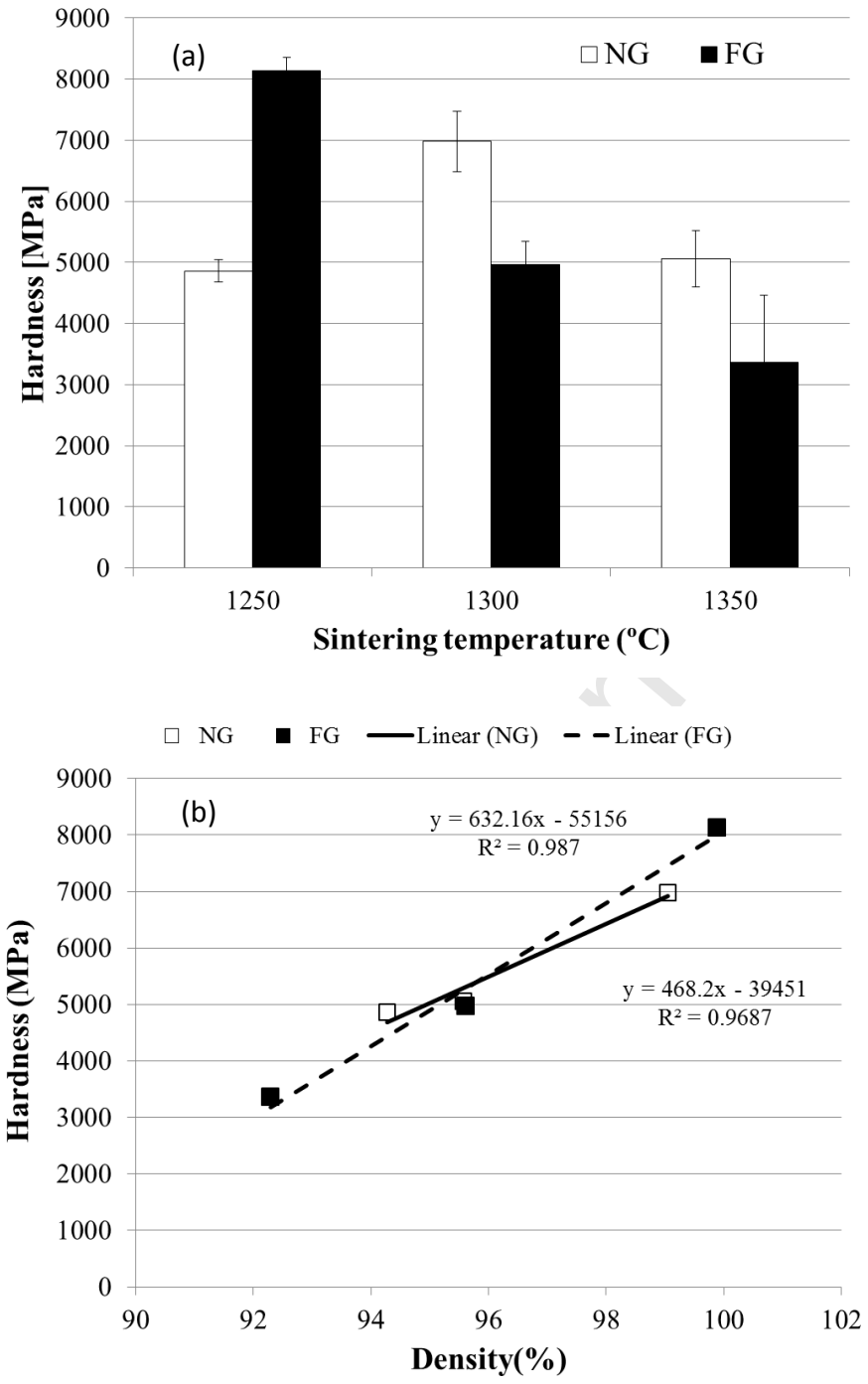

Figure 5

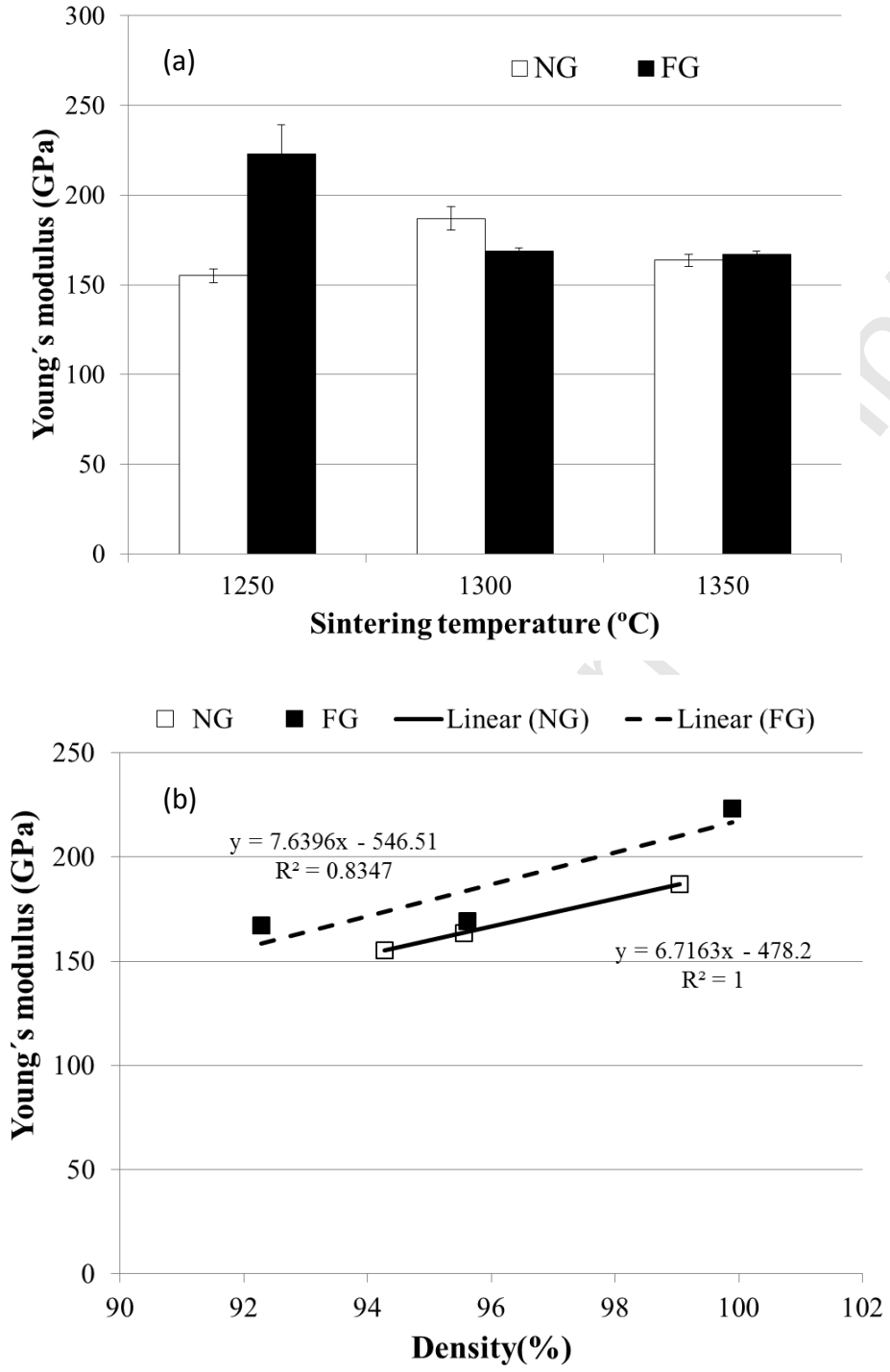

Figure 6

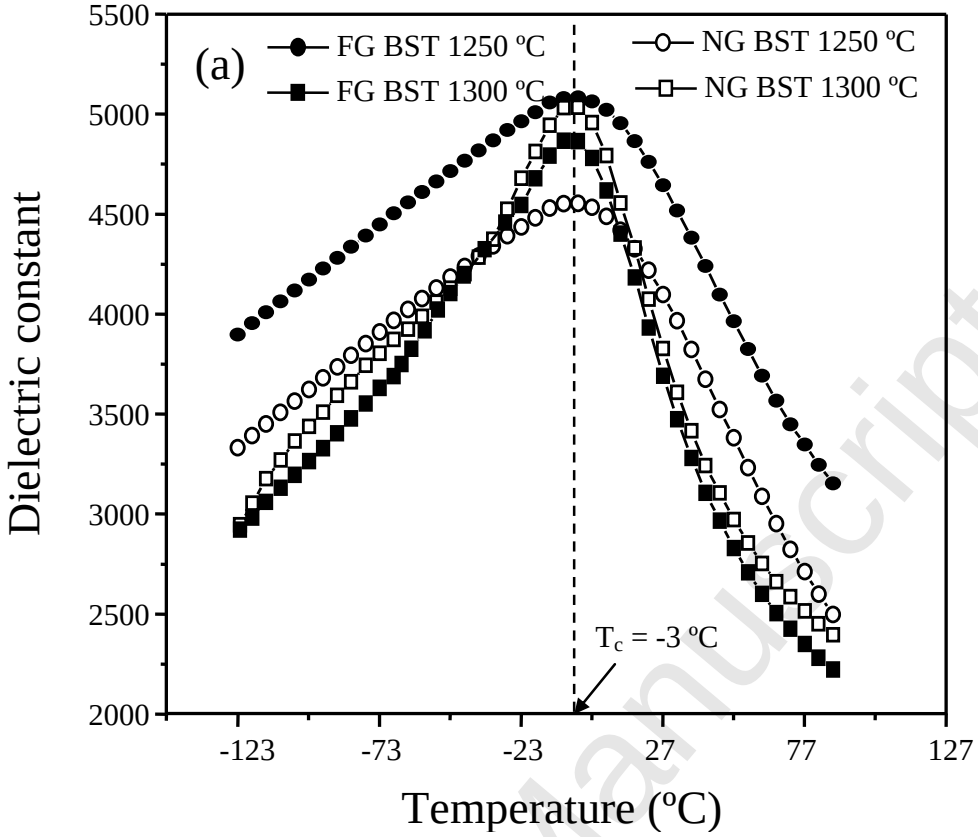

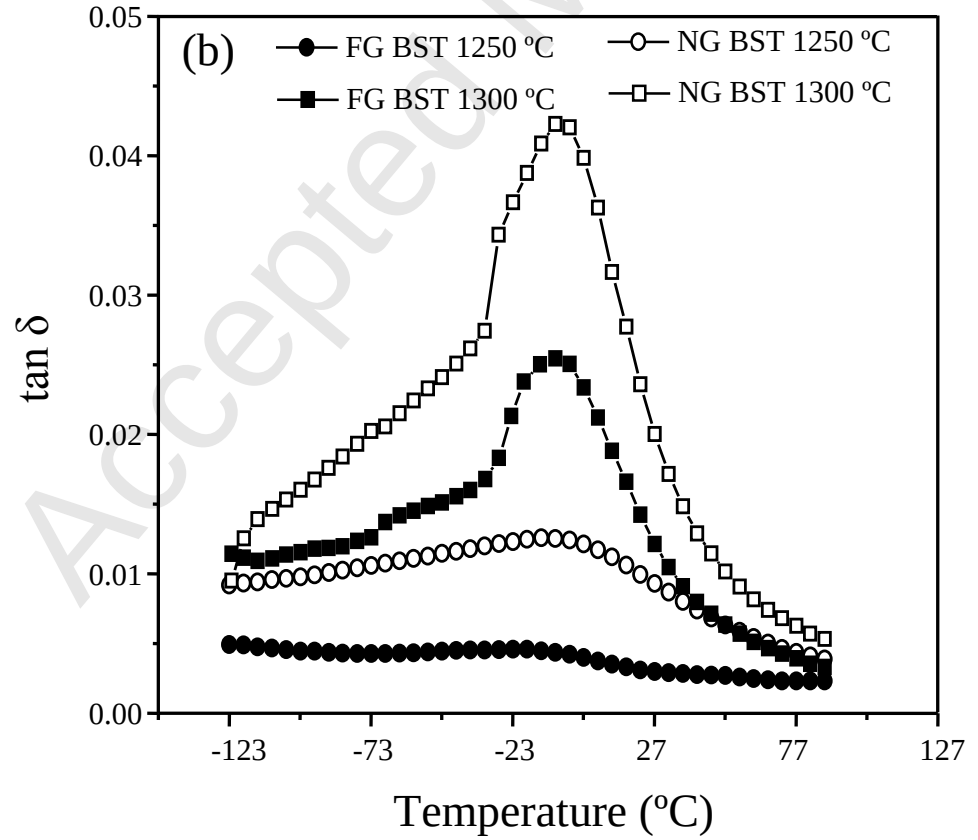

Figure 7

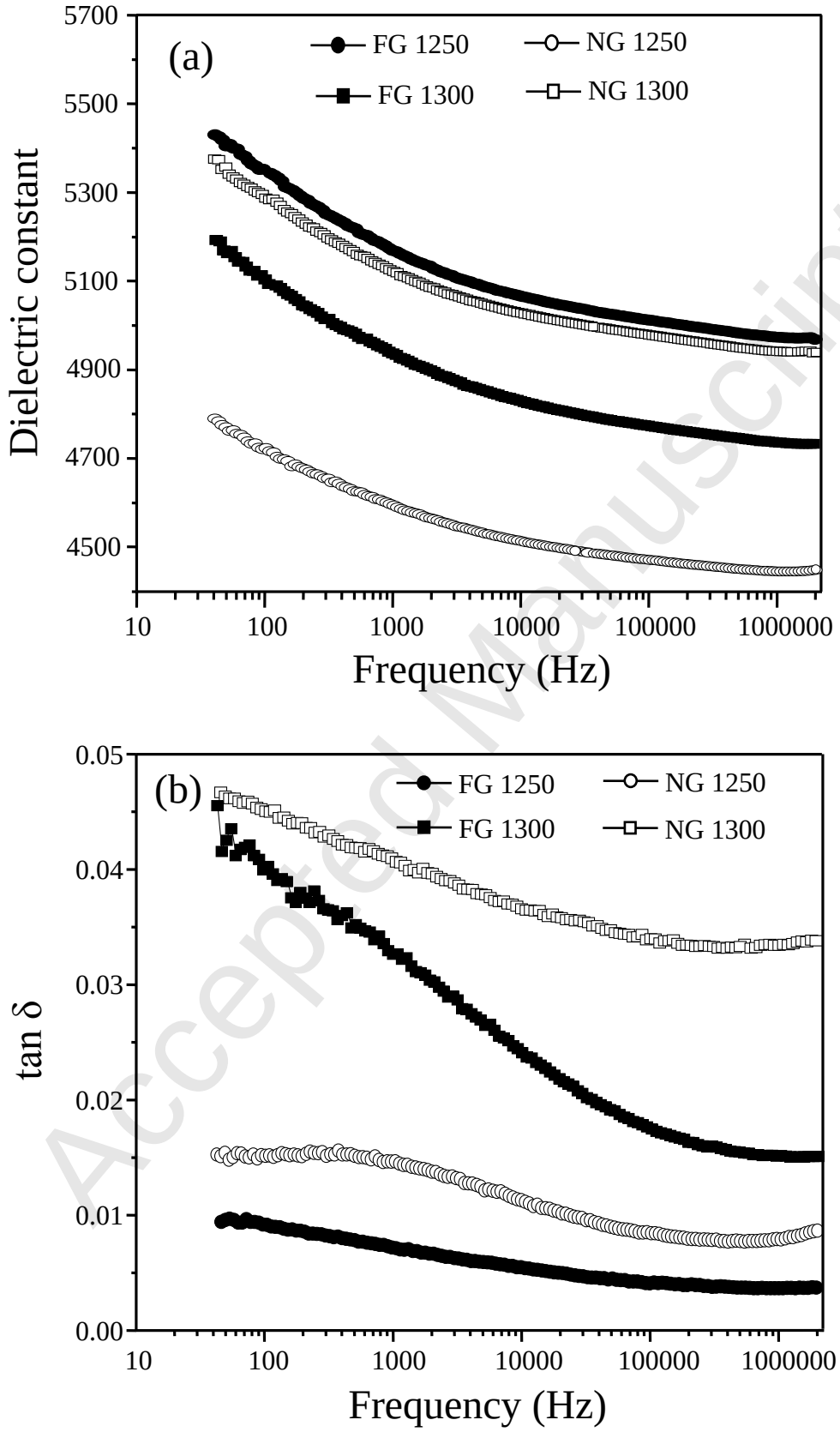

Figure 8